Dynamics of Argon Collisions with Water Ice: Molecular Beam Experiments and Molecular Dynamics Simulations

Patrik U. Andersson,[†] Mats B. Någård,[†] Kim Bolton,[†,‡] Marcus Svanberg,[†] and Jan B. C. Pettersson*[,†,§]

Department of Chemistry, Physical Chemistry, Göteborg University, S-412 96 Göteborg, Sweden, School of Engineering, University of Borås, SE−501 90 Borås, Sweden, and School of Environmental Sciences, Göteborg University, S-412 96 Göteborg, Sweden

Received: October 5, 1999; In Final Form: January 4, 2000

The dynamics of argon atom collisions with water ice at 110−180 K is investigated using molecular beam experiments and molecular dynamics simulations. Initial argon energies of 0.065 to 0.93 eV and incident angles of 0 to 70° are used, and directly scattered and thermally desorbed atoms are separated by angular-resolved time-of-flight measurements. For thermal incident energies the scattering is almost entirely due to trapping followed by thermal desorption. For higher energies direct inelastic scattering is observed, and the scattering channel is favored by a high initial energy, a large incident angle and a high surface temperature. Results from simulations are found to agree well with experimental data, although the simulations overestimate the energy transfer by approximately 10%. The results confirm that Ar collisions with ice surfaces are highly inelastic and characterized by very effective transfer of energy to surface modes. This indicates that molecules with a mass similar to Ar will trap on the surface of water ice particles with a high probability under stratospheric conditions.

1. Introduction

Ice particles play an important role for the chemistry of the atmosphere by providing surfaces where heterogeneous reactions may proceed. They may also act as a sink for molecules and thereby alter the gas-phase concentrations. One important example is the seasonal depletion of ozone in the stratosphere over the polar regions, where the inactive reservoir molecules HCl and $ClONO_2$ are converted to Cl_2 and HOCl on stratospheric ice particles. These species are photolyzed when the sun returns to the region in the spring, which produces Cl radicals that subsequently attack ozone.[1]

The collision and accommodation of molecules on a surface is the first step in any heterogeneous process. During a collision with an ice surface a molecule can trap on the surface, directly scatter back into the gas phase, or perhaps penetrate the surface and diffuse into the bulk of the ice. Trapped molecules may thermally desorb from the surface, diffuse in the surface layer or into the bulk, or form chemical bonds. Scattering from single-crystal surfaces has been studied extensively during the past 40 years using molecular beam techniques,[2,3] while scattering from molecular surfaces, such as ice, has not been studied to the same extent.

Glebov et al.[4] and Braun et al.[5] scattered He atoms from crystalline ice surfaces grown at 125 K. Diffraction measurements at a surface temperature of 30 K showed enhanced vibrational amplitudes at the surface and a large multiphonon background, which are consistent with dynamic disorder and a large accommodation coefficient at the surface. Gotthold and Sitz[6] studied the scattering of N_2 from ice at 100−150 K with state-resolved detection of the flux from the surface. For beam incidence in the surface normal direction, the outgoing flux was found to be entirely dominated by trapping−desorption for kinetic energies below 0.3 eV. Inelastic scattering was observed at higher incident energies, with a direct scattering probability reaching 23% at 0.75 eV. The molecules in the scattering channel lost up to 85% of their incident energy in the surface collision. Molecular beam scattering has also been used to determine the sticking probability for molecules on water ice surfaces. Brown et al.[7] determined a sticking coefficient, S_0, of 0.99 ± 0.03 for H_2O on ice, independent of incident kinetic energy (0.04−1.7 eV) and incident angle (0−70°). Rieley et al.[8] measured sticking coefficients of 0.95 ± 0.05 for HCl and 1.00 ± 0.05 for HBr using thermal molecular beams colliding with ice at 80−130 K, and Isakson and Sitz[9] obtained $S_0 = 0.91 \pm 0.06$ for HCl on ice at 120−125 K. Related to the work on scattering from ice surfaces are the experimental studies of the accommodation of molecules on large water clusters by Whitehead and co-workers.[10−12]

Molecular dynamics (MD) simulations have also been carried out for a few molecule−ice systems. Classical MD simulations of HCl and HOCl colliding with ice surfaces by Clary and Kroes[13] gave unity sticking coefficients under thermal conditions. The same result was obtained from a mixed quantum-classical treatment of HCl on ice by Wang and Clary.[14] A recent MD study of Al-Halabi et al.[15] showed that HCl may penetrate the ice surface at high incident energies and small incident angles. Bolton et al.[16] have recently performed classical MD simulations on Ar scattering from ice and found that the initial kinetic energy is effectively taken up by the surface and rapidly removed from the impact site. Bolton and Pettersson[17] have also characterized the trapping−desorption and thermal surface penetration channels and found that up to 36% of the argon atoms penetrate the ice surface and diffuse into subsurface interstitial sites as a result of thermally produced disorder in the topmost ice bilayer. The trapping−desorption channel could

* To whom correspondence should be addressed. Telephone: +46.31.772 28 28. Fax: +46.31.772 31 07. E-mail: janp@phc.chalmers.se.

10.1021/jp9935440 CCC: $19.00 © 2000 American Chemical Society
Published on Web 03/04/2000

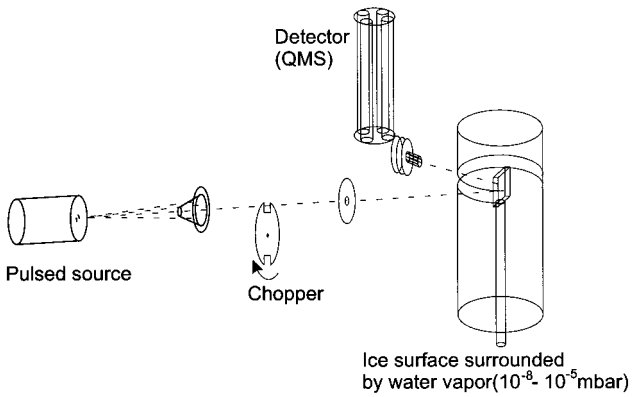

Figure 1. A schematic representation of the surface scattering apparatus used in the experiments.

be described by first-order kinetics, with a rate constant of 2.1×10^{10} s^{-1} at a surface temperature of 180 K.

These previous studies show that trapping or sticking coefficients are, in general, very high for molecular collisions with ice surfaces. Surface modes are efficiently excited at impact, which leads to a large energy loss for directly scattered molecules. The available experimental information is, however, rather limited, and there is a need for additional experimental data in order to improve the understanding of the dynamics of molecule−ice interactions. In this paper, we present experimental results from molecular beam experiments of argon atom scattering from crystalline ice. A newly developed experimental setup allowed us to perform experiments in the temperature range 110−180 K, close to the temperatures of relevance to stratospheric chemistry (≥ 185 K). Angular-resolved time-of-flight distributions are measured for different incident kinetic energies (0.065, 0.43, and 0.93 eV) and incident angles (0−70°), and the experimental data are compared with classical MD simulations. Argon has a concentration of about 1% in the atmosphere, and is not in itself of great importance for the heterogeneous chemistry in the atmosphere. However, the mass of argon, 40 amu, is similar to the masses of other molecules present in the atmosphere such as HCl (36 amu) and HOCl (52 amu). The mass of the molecule is a critical factor for the efficiency of energy transfer and trapping,[16] and the Ar−ice system serves as a model for more complex molecular systems.

2. Experimental Section

2.1. Scattering Apparatus. The Ar−ice scattering experiments are performed in a vacuum apparatus designed to work at ice surface temperatures up to at least 180 K. It is illustrated in Figure 1. A pulsed solenoid valve molecular beam source (General Valve) is positioned in the first chamber and mounted on a manipulator allowing *x*-, *y*-, and *z*-translation for accurate alignment. Molecules expand through an orifice with a diameter of 0.2 mm, and pulses of typically 220 μs duration are generated at a frequency of 60.7 Hz, giving a pressure of $1-6 \times 10^{-4}$ mbar in the first chamber. The first chamber is pumped by a 3000 L/s oil-diffusion pump backed by an 80 L/s roots pump followed by a 30 m^3/h two-stage rotary-vane pump. The flux generated by the pulsed source enters the second chamber through a skimmer with an opening of 0.5 mm. The pulses are chopped in the second chamber by a rotating disk with two slits (3.3% duty time) in order to select the central part of each pulse. The chopper is rotated at 182 Hz and synchronized with the pulsed valve, giving square wavelike beam pulses with a width of 90 μs. Three different gas mixtures are used: Pure argon, 5% Ar in He, and ∼2% Ar in H_2, which gives the argon atoms translational energies of 0.065, 0.43, and 0.93 eV. In the case of pure argon, the source pressure is kept at 1.6 bar in order to avoid clustering (dimers = 0.6% of monomers), whereas clustering is negligible at pressures below 9 bar for the gas mixtures. The beam enters the third chamber through a 1 mm aperture. This chamber is pumped by three turbomolecular pumps (total pumping speed: 900 L/s), one liquid helium pumped cryostat (pumping speeds: N_2, 460 L/s; H_2O, 6800 L/s; Ar, 370 L/s), and liquid nitrogen cooled surfaces (0.16 m^2). The upper part of the third chamber consists of a differentially pumped rotatable flange. On this flange a quadrupole mass spectrometer (QMS) (ABB Extrel, model MEXM0500) is positioned. The mass spectrometer is differentially pumped by a 270 L/s turbomolecular pump in order to decrease the background signal of argon. The pressure in this differentially pumped chamber was typically 1×10^{-9} mbar during scattering experiments. For beam measurements, the QMS can be positioned both 397 and 783 mm downstream from the chopper by 180° rotation of the top flange. This eliminates systematic errors due to the flight time in the quadrupole and the chopper opening time, giving more accurately determined velocities. The rotation of the top flange makes it possible to perform time-of-flight measurements in different surface scattering directions in the plane defined by the beam and the surface normal. The atoms enter the ionizing part of the QMS through a 3 mm orifice positioned 180 mm from the surface, which gives an angular resolution of less than ±1.5°. The atoms are ionized by electron bombardment from a filament, positioned 193 mm from the graphite surface. The mass-filtered ions are detected and the pulses from the electron multiplier are counted and stored on a multichannel scaler with a dwell time of 10 μs, and typically 10 000 pulses are fired.

A cylinder with a diameter of 90 mm is mounted on the bottom of the third chamber. A surface holder which is mounted on a five dimensional surface manipulator (three translations and two rotations), is positioned inside the cylinder. A 12 × 12 mm graphite surface (Advanced Ceramics Corp., grade ZYB) is mounted on the manipulator. The surface holder can be cooled by liquid nitrogen and heated by irradiation, giving a surface temperature range of 100−750 K with fluctuations less than 0.2 K. The temperature is measured by a thermocouple clamped 7 mm from the surface center. A slit opening (height: 7 mm, width: 200 mm) in the cylinder allows the argon beam to impinge on the ice surface and the scattered atoms to reach the detector. By introducing the cylinder we can maintain a low pressure in the third chamber (4×10^{-9} to 1×10^{-7} mbar) while the ice surface is surrounded by a high partial water vapor pressure ($\leq 3 \times 10^{-5}$ mbar).

2.2. Ice Surface Buildup. Ice surfaces are prepared by deposition of water vapor, which was introduced to the surface through a leak valve. The water was of Millipore quality and stored in a stainless steel container. It was further purified by several freeze−pump−thaw cycles. The water vapor pressure around the surface was adjusted so that an ice surface on the graphite substrate was built up at a speed of about 2 monolayers per second (ML/s). The initial ice surface buildup was always performed at a temperature of 150 K, which produces stable crystalline ice I. Ice I exists in two forms, cubic and hexagonal ice,[18] of which the hexagonal phase is the most thermodynamically stable form at all temperatures, but often cubic ice is initially formed at a temperature of 150 K.[19] Two important factors that determine the type of ice formed are the deposition rate and the substrate used for initial condensation. The relatively fast deposition rate used for ice buildup in this study makes it

likely that cubic ice is produced at temperatures of 150 K and below during the time of our measurements. The surface and bulk structures of the two phases are, however, very similar.

The ice thickness is measured by detecting the reflectance of a laser beam (1 mW, 670 nm diode laser) directed at the ice/graphite surfaces with an incident angle of 5° with respect to the surface normal. The sinusoidal intensity profile of scattered light during ice buildup was recorded by a diode and used to deduce the ice thickness.[20] After condensation of about 400 ML, the water pressure is decreased to give a condensation rate of about 0.5 ML/s. This condensation rate is maintained during surface scattering measurements to exclude any contamination by residual hydrocarbons or carbon monoxide. When ice surface temperatures of 110 K are required, the water inlet is turned off before cooling the ice surface from 150 K. This prevents formation of an amorphous phase.[21] Measurements were performed to ensure that the scattering intensity was not affected by impurities during the time span of the experiments. Ice surfaces at 180 K are prepared in a different way: An ice surface is initially constructed at 150 K as explained above. The water pressure and surface temperature are then increased in steps, until a stable surface is obtained at 181 K. Finally the surface is cooled to 180 K, giving a surface construction rate of about 2 ML/s. Attempts to start the ice surface construction at 180 K resulted in a highly diffusive light scattering and a large decrease in measured light intensity, which made it difficult to monitor the ice surface buildup. This decrease in light scattering has been studied previously[22] and has been interpreted as being due either to cracking of the ice or the conversion from cubic to hexagonal ice.

3. Simulation Methods

The experimental studies have been complemented with MD simulations of Ar scattering from ice. The potential energy surface (PES) used to simulate the trajectories is described elsewhere.[16] The H_2O molecules are rigid and their pairwise intermolecular interactions are represented by the TIP4P potential.[23] The Ar−ice interaction is the sum over all Ar−H_2O interactions, where each interaction is approximated by an isotropic Lennard-Jones 12−6 potential with a well depth of 0.015 eV and an Ar−H_2O minimum energy separation of 3.37 Å. An isotropic representation of the interaction is expected to be valid for the Ar−H_2O collision energies investigated here,[24,25] but a nonisotropic PES[26] would be required for higher energies. All intermolecular potentials are multiplied by a switching function, which smoothly adjusts the intermolecular forces to zero for separations larger than 10 Å.

Collisions between Ar atoms and the basal (0001) plane of an infinitely large ice Ih surface were simulated using an ice slab with periodic boundary conditions in the surface plane. The ice slab, which comprises 8 bilayers with 96 water molecules in each bilayer, is based on the optimized hexagonal structure determined by Hayward and Reimers.[27] The ice surfaces were thermalized at 110, 150, or 180 K by integrating the H_2O molecular coordinates for at least 500 ps. This is sufficient time for convergence of the rotational and vibrational temperatures, and allows for reconstruction of the top surface bilayer.[17] When integrating the trajectories the molecular positions of the lowest two (seventh and eighth) ice bilayers were fixed to maintain the ice Ih bulk structure. The molecular coordinates of the adjacent (sixth) bilayer were integrated using the Langevin equation,[28] which approximately includes frictional and stochastic coupling of this bilayer with the bulk ice. The water molecules in the five uppermost bilayers were integrated using the Verlet algorithm modified for rigid body motion.[29] A step size of 6 fs was used. In the absence of temperature coupling energy was conserved to four significant figures. The Ar−ice collisions were initiated with the Ar atom located ≈10 Å above the thermalized surface, where the Ar−ice intermolecular force is zero. The Ar was randomly placed at any point above the ice surface and propagated toward the surface with a specified initial energy E_i and incident angle θ_i. Ensembles of at least 3200 trajectories were propagated, where each trajectory simulated a new Ar−ice collision. Scattering trajectories were terminated when the Ar−ice separation increased to 10 Å after a collision. Nonscattering collisions were terminated when the Ar−ice energy was less than the Ar−ice well depth and the Ar molecule had a thermal kinetic energy. At this stage, the Ar was considered to be trapped on the surface.[16] The ensemble results were analyzed to get trapping probabilities, angular scattering distributions and distributions of the final Ar energy, E_f. The methods used for the analyses have been described previously.[16]

4. Results

4.1. Experimental Results. We have studied the dynamics of argon collisions with crystalline ice by varying the argon incident kinetic energy, surface temperature, and incident angle. Figure 2 shows time-of-flight spectra of argon scattering from an ice surface at 150 K with an incident kinetic energy of 0.43 eV. The incident angle was 70° with respect to the surface normal, and data are displayed for five different scattering directions. The spectra show a sharp and fast peak on top of a broader and slower component. The relative intensity of the two components changes substantially with scattering angle; the fast peak dominates at large scattering angles, while the slower component increases when moving toward the surface normal direction. The distribution at $\theta_f = 0°$ is essentially the result expected for thermal desorption from the 150 K ice surface, and the same result is observed in backward scattering directions (not shown). The data have been fitted by a sum of two components corresponding to trapping−desorption and direct inelastic scattering. The velocity distribution for thermally desorbed atoms is

$$F_{TD}(v) = c_1 v^2 \exp(-mv^2/2k_B T_1) \quad (1)$$

where v is the velocity, c_1 is a scaling factor, m is the argon mass, and T_1 is the temperature. The velocity distribution of the inelastically scattered atoms has the form

$$F_{IS}(v) = c_2 v^2 \exp(-m(v - v_0)^2/2k_B T_2) \quad (2)$$

where c_2 is a scaling factor, v_0 is a drift velocity and T_2 is a temperature describing the width of the velocity distribution. The distributions take into account that the mass spectrometer is density sensitive. The sum of eqs 1 and 2 has been fitted to the experimental results by varying c_1, c_2, v_0, and T_2, while keeping T_1 constant at the surface temperature. The beam intensity profile at the surface has a width of about 100 μs, and this has also been taken into account by convoluting over the beam profile. The fitted distributions obtained from eqs 1 and 2 and their sum are included in Figure 2. The excellent agreement between fits and experimental data is typical for all conditions used in this paper.

The quality of the fits to the experimental data indicates that the surface residence time is negligible under the conditions used in this study. Based on the experimental time resolution, we conclude that the residence time is below 30 μs for all cases

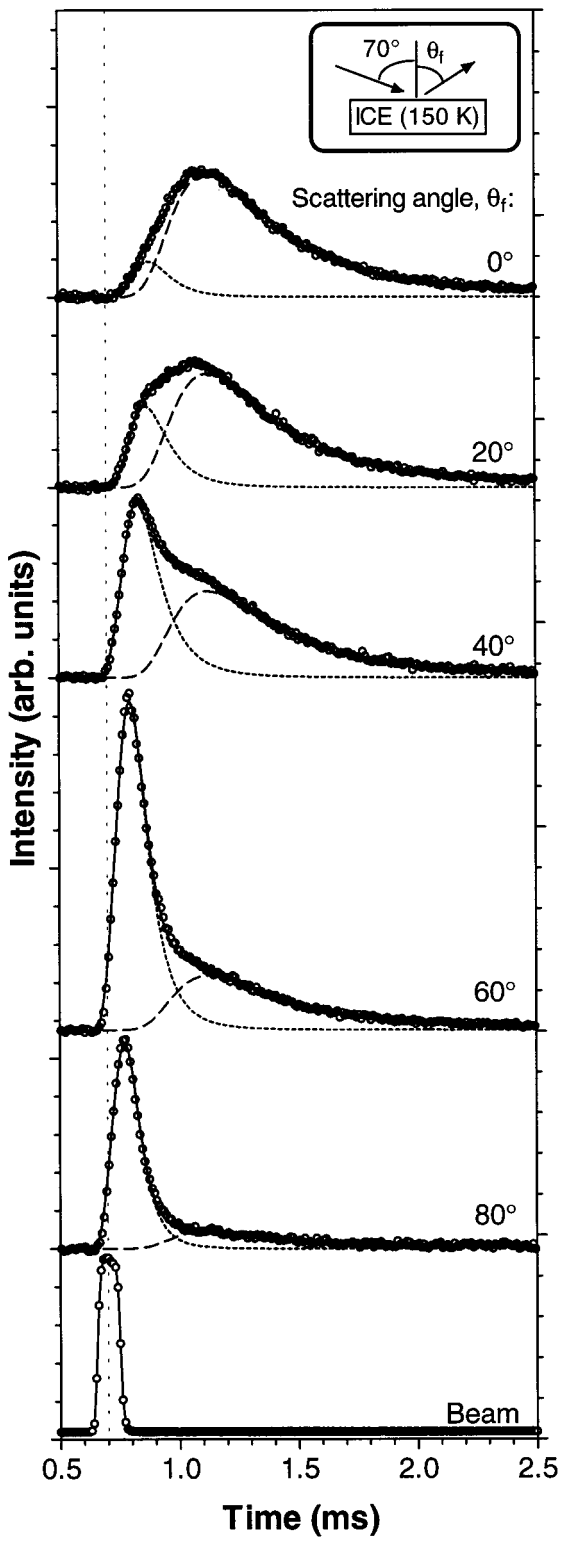

Figure 2. Time-of-flight spectra for 0.43 eV Ar scattering from ice. Experiments (○), fit (—), inelastic scattering (···), and thermal desorption (– – –). The surface temperature was 150 K and the incident angle 70°. The scattering angles are indicated in the figure. The beam measurement is obtained by moving the surface out of the beam and corresponds to elastic scattering. The dashed vertical line is included to guide the eye.

investigated here. MD simulations[17] have shown that for a surface temperature of 180 K, 99.9% of all trapped Ar atoms leave the ice surface within 0.3 ns after surface impact. These short residence times cannot be resolved experimentally in this study.

The results from time-of-flight spectra have been used to construct angular distributions for the direct scattering and trapping−desorption channels. The angular distributions obtained experimentally have also been transformed into a flux in order to compare with the results from molecular dynamics simulations (see below). Data for the same conditions as in Figure 2 are shown in Figure 3a. A cosine angular distribution is, as expected, obtained for thermally desorbed atoms. The distribution for directly scattered atoms peaks close to the specular direction, but is broad and extends toward the surface normal direction. Figure 3b shows the average kinetic energy of the inelastically scattered atoms. The atoms lose 50−80% of their incident energy during surface contact, and energy transfer depends sensitively on the scattering angle. The fastest atoms recoil at angles close to the surface tangential direction, and the final kinetic energy then decreases when going toward the surface normal direction, indicating that atoms do not conserve momentum parallel to the surface.

Angular distributions observed using incident energies of 0.065, 0.43, and 0.93 eV are compared in Figure 4a. For the lowest (thermal) energy, no directly scattered atoms could be resolved in the experiments and the flux from the surface is well described by a cosine distribution due to trapping−desorption. For the higher energies, the inelastic scattering intensity increases and, when going from 0.43 to 0.93 eV, the distribution width decreases. Figure 4b shows that energy loss is even more dramatic for an incident energy of 0.93 eV, increasing from about 50% at large angles to 90% for backward scattering angles.

The effect of incident angle has been studied for a kinetic energy of 0.43 eV and a surface temperature of 150 K. As seen in Figure 5, the trapping−desorption probability increases for smaller incident angles. The inelastic scattering distributions become very broad for incident angles of 20 and 45°, and the energy loss is even more pronounced and shows less dependence on scattering angle than observed for $\theta_i = 70°$. The effect of surface temperature on the scattering from crystalline ice is shown in Figure 6. The angular distributions observed for surface temperatures of 110, 150, and 180 K have similar shapes, but the inelastic scattering intensity is larger for a temperature of 180 K. There are no large differences in the angular-resolved final kinetic energy between the three cases, as shown in Figure 6d−f.

We have also measured the trapping probability for Ar (0.43 eV) as a function of incident angle. The trapping probability cannot be determined directly by comparing the flux in the trapping−desorption and direct scattering channels, since the out-of-plane distribution is not known for the inelastically scattered component. The trapping probability was instead determined in the following way: time-of-flight spectra measured at a scattering angle of 40° were used to determine the flux in the trapping−desorption channel (normalized to the beam flux). This flux was then compared with the flux obtained for Ar scattering with an initial energy of 0.065 eV (again normalized to the beam flux), where the trapping−desorption probability is unity. The ratio between these fluxes gives the trapping probability. Figure 7 shows that the trapping probability is always high with a maximum value of 0.85 at normal incidence, which decreases to 0.60 for an incident angle of 70°.

4.2. Comparison With Molecular Dynamics Simulations. In Figure 3, experimental and simulation results are compared for Ar (0.43 eV) scattering from the ice surface (150 K) with $\theta_i = 70°$. Thirty thousand trajectories were calculated for these conditions. Figure 3a shows simulated angular distributions for

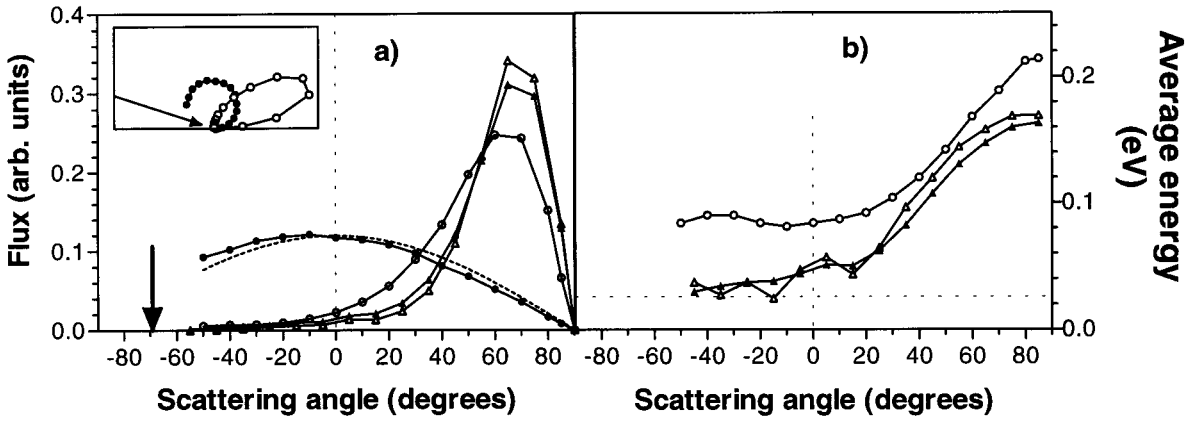

Figure 3. (a) Experimental angular distributions for thermal desorption (●) and inelastic scattering (○), and MD simulations using an out-of-plane window of ±10° (△) and ±90° (▲). A cosine distribution (···) is included for comparison. The results are also shown as a polar plot (inset). The MD-simulated distribution is area normalized to the experimental inelastic distribution. (b) Average translational energy of the inelastically scattered atoms, experiments (○), and MD simulations using an out-of-plane window of ±10° (△) and ±90° (▲). The dashed horizontal line corresponds to $2k_BT_S$. The conditions are the same as in Figure 2.

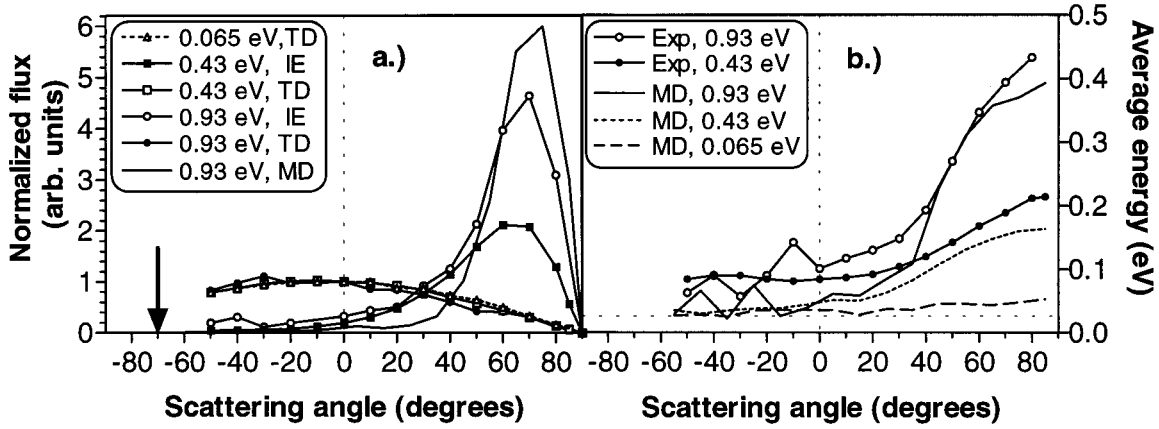

Figure 4. (a) Angular distributions for three different incident energies: 0.065, 0.43, and 0.93 eV. The incident angle was 70° and the ice surface temperature was 150 K. The experimental intensities are normalized to unity for thermal desorption in the surface normal direction. (b) Average energies for inelastically scattered atoms. TD = thermal desorption, IE = inelastic scattering, and MD = molecular dynamics simulations. The incident kinetic energies are indicated in the panels.

two different choices of the out-of-plane window: ±10° and ±90°. Of the total 30 000 trajectories, 11% scatter inelastically within the ±10° window and 30% scatter within ±90°. These two out-of-plane windows give very similar angular and average kinetic energy distributions, as shown in Figure 3b. We have therefore chosen to use all scattered trajectories (±90°) for other conditions where about 5000 trajectories were simulated. The simulated angular distributions in Figure 3a show the same qualitative features as the experimental data, but the widths of the simulated distributions are somewhat smaller and the peak is slightly shifted toward the tangential direction. The thermally equilibrated atoms in the simulations are not included in the results in Figure 3. The simulated energy distributions in Figure 3b also show the same trend as the experimental data, with a decrease in scattering energy when moving toward the surface normal direction, but the simulations slightly overestimate the energy transfer for all scattering angles.

The simulations reproduce the qualitative effect of incident kinetic energy on the angular and velocity distributions. The results for a kinetic energy of 0.93 eV, given in Figure 4, show the same deviations from the experimental data as observed for 0.43 eV. For the lower translational energy of 0.065 eV, 4% scatter inelastically in the simulations while no direct scattering was observed experimentally. As shown in Figure 5a−b, when the incident angle is decreased to 20 and 45°, the angular distributions are well reproduced by the MD simulations, while the simulations continue to overestimate energy loss to the surface (Figure 5d−e). Comparisons made at different surface temperatures (Figure 6a−c) again show qualitative agreement between experiments and simulations. A detailed comparison, however, shows that the simulated angular distributions become broader with increasing surface temperature, which may be explained by an increased thermal movement of the surface molecules, while the opposite trend is found experimentally. The trapping probability is found to be slightly higher in the simulations, as illustrated in Figure 7, which is consistent with the higher degree of energy transfer in the simulations.

5. Concluding Remarks

To summarize, the results for argon scattering from water ice show that the surface collisions are highly inelastic, and that thermal desorption dominates for incident kinetic energies below 1 eV. For thermal kinetic energies the trapping probability is essentially unity, while a direct scattering channel opens at higher incident energies. The energy loss to the surface is substantial for the direct scattering channel, reaching values of up to 90% depending on the collision conditions. The energy loss is largest perpendicular to the surface, but also the energy loss parallel to the surface plane is large under all conditions studied here. The efficient uptake of energy by the surface is also consistent with the large trapping probabilities observed.

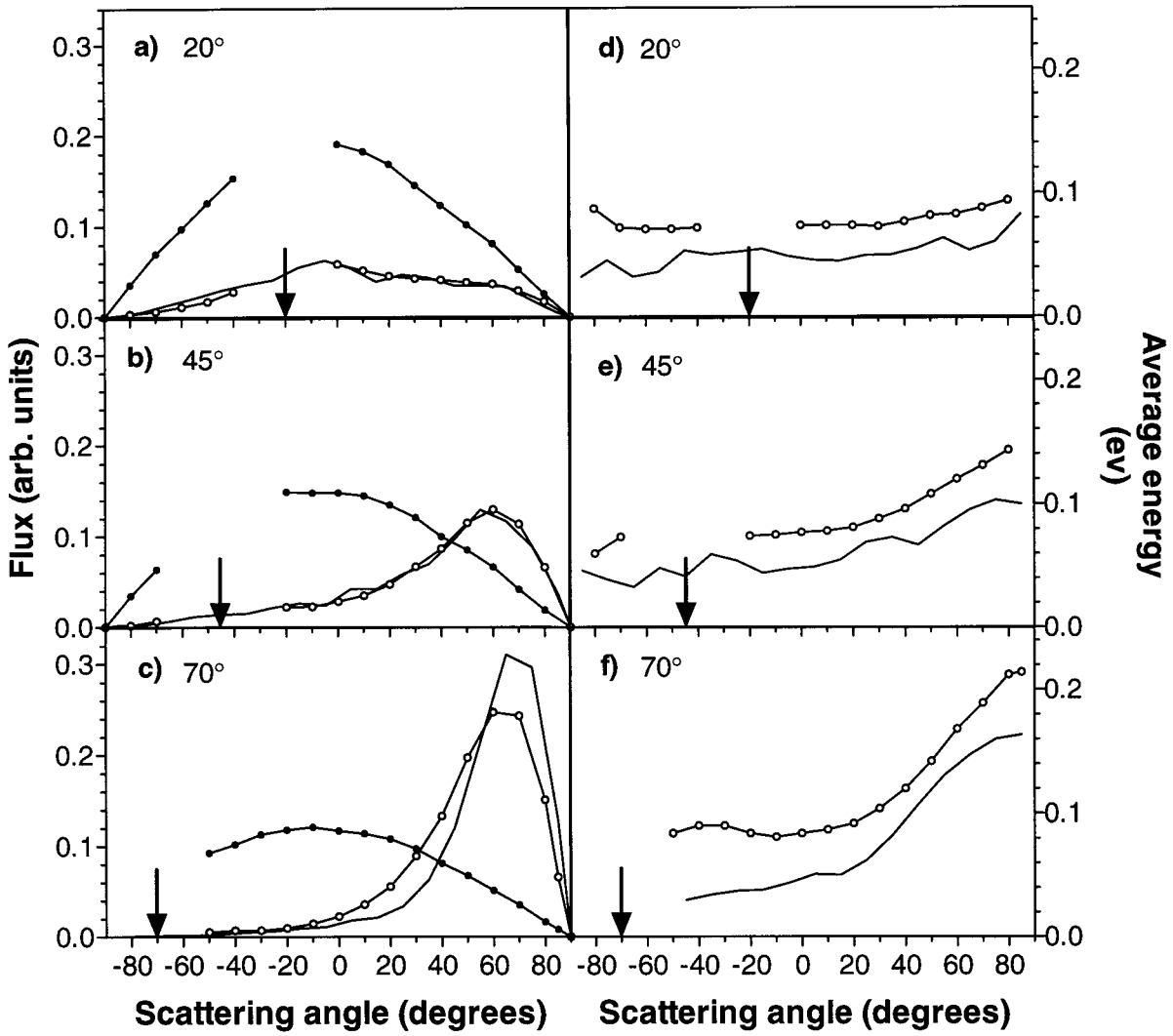

Figure 5. (a−c) Angular distributions for three different incident angles: 20, 45, and 70°. The incident energy is 0.43 eV and the ice surface temperature is 150 K. Thermal desorption (●) and inelastic scattering: experiments (○) and MD simulations (—). (d−f) corresponding average energies.

The results are consistent with earlier studies of ice surfaces concerning the large probability for molecular trapping and sticking. In particular, the data agree well with the results for N_2 scattering from ice by Gotthold and Sitz.[6] For normal incidence, they observed an energy loss of 85% for inelastically scattered molecules and a trapping probability of 0.77 for an incident energy of 0.75 eV, in good agreement with the corresponding data for the Ar−ice system. Previous MD simulations[16] have also shown that the trapping probability for Ar on ice is large for all surface temperatures between 0 and 300 K. These results indicate that the trapping probability for molecules, with masses similar to or larger than Ar, on water ice surfaces, should be large under all conditions of relevance for atmospheric chemistry. This is of great importance for the rates of heterogeneous reactions on ice surfaces in the atmosphere, as well as other phenomena including particle growth and particle mobility in air.

The decrease in final kinetic energy with decreasing scattering angles (i.e., toward the surface normal direction) is opposite to the trend generally found for scattering from metal surfaces[2,3,30] and graphite surfaces[31] in the same kinetic energy range. These systems generally conserve the scattering particle's kinetic energy parallel to the surface plane better than is observed for ice. The trends observed in this study resemble the results obtained for scattering from liquid surfaces by Nathanson and co-workers,[32,33] although the degree of energy loss is larger in the present case.

The MD simulations of Ar atom collisions with ice show qualitative, and in some cases semiquantitative, agreement with the experimental angular distributions. The simulations also give the same trends as experimental data concerning energy transfer, but systematically overestimate the degree of energy transfer by 10−20%. The current study supports the collision dynamics seen in the MD simulations of the Ar−ice system,[16,17] and the reader is referred to these papers for details.

We have not attempted to refine the potential energy surface in order to obtain better agreement between the simulation and experimental data. It is also possible that quantum effects cause the deviations between theory and experiments, considering the low mass of the surface molecules and high frequency surface modes. Some of the discrepancy between experiment and simulation results may also be explained by deviations of the experimental ice surface from a single crystal structure. Ledges and mismatches on the surface should affect the results more at larger incident angles, and the deviations from the experimental results are, in fact, highest for the largest incident angle of 70°. Comparing the final kinetic energies at negative scattering angles, we believe that the higher energy obtained experimentally may partly be due to backscattering from ledges and mismatches. Further experiments and calculations with

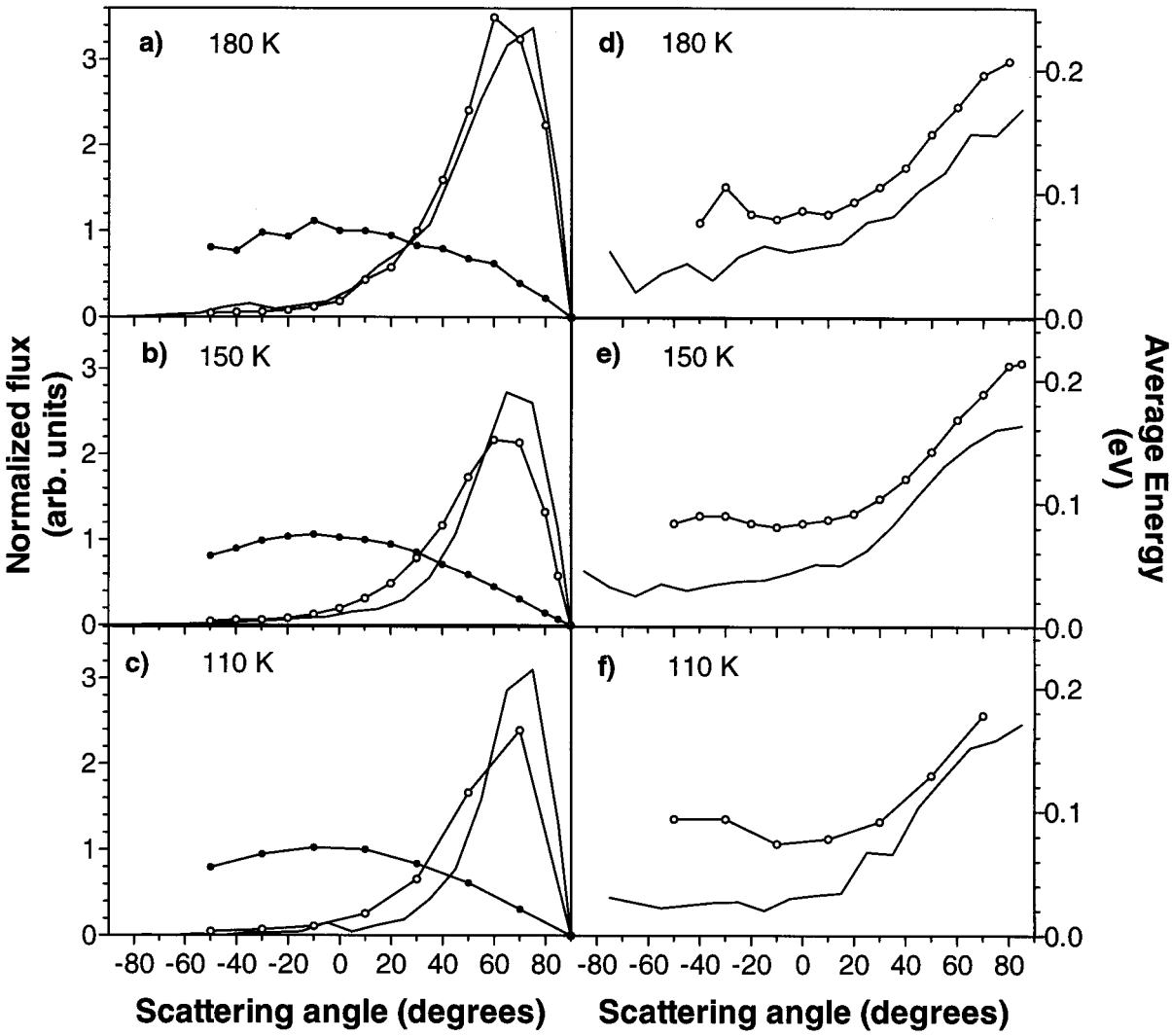

Figure 6. (a−c) Angular distributions for three different surface temperatures: 110, 150, and 180 K. The incident energy is 0.43 eV and the incident angle is 70°. Thermal desorption (●) and inelastic scattering: experiments (○) and MD simulations (—). The experimental intensities are normalized to unity for thermal desorption in a scattering direction of 10°. (d−f) corresponding average energies.

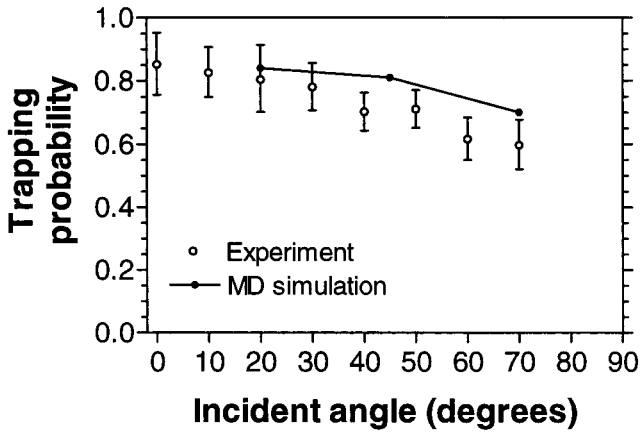

Figure 7. Trapping probability as a function of incident angle: experimental data (○) and MD simulations (●). The translational energy of the argon atoms was 0.43 eV and the surface temperature was 150 K.

crystalline and amorphous surfaces formed under different conditions may help to clarify this question.

We conclude that the experimental setup used in this study allows for detailed molecular beam experiments at elevated surface temperatures which requires relatively high partial pressures of water outside the ice surface. The technique has been employed to study the more complex scattering of HCl from ice, and the results will appear in a subsequent paper.

Acknowledgment. We gratefully acknowledge the construction work and technical support of Mr. Benny Lönn. This project was supported by the Swedish Natural Science Research Council. K.B. is grateful to the Adlerbertska Forskningsfonden for financial support.

References and Notes

(1) Molina M. J.; Tso, T.-L.; Molina, L. T.; Wang, F. C. Y. *Science* **1987**, *238*, 1253.

(2) Goodman, F. O.; Wachman, H. Y., Eds.; *Dynamics of Gas−Surface Scattering*; Academic Press: New York, 1976.

(3) Rettner, C. T.; Auerbach, D. J.; Tully, J. C.; Kleyn, A. W. *J. Phys. Chem.* **1996**, *100*, 13021.

(4) Glebov, A.; Graham, A. P.; Menzel, A.; Toennies, J. P. *J. Chem. Phys.* **1997**, *106*, 9382.

(5) Braun, J.; Glebov, A.; Graham, A. P.; Menzel, A., Toennies, J. P. *Phys. Rev. Lett.* **1998**, *80*, 2638.

(6) Gotthold, M. P.; Sitz, G. O. *J. Phys. Chem. B* **1998**, *102*, 9557.

(7) Brown, D. E.; George, S. M.; Huang, C.; Wong, E. K. L.; Rider, K. B.; Smith, R. S.; Kay, B. D. *J. Phys. Chem.* **1996**, *100*, 4988.

(8) Rieley, H.; Aslin, H. D.; Haq, S. *J. Chem. Soc., Faraday Trans.* **1995**, *91*, 2349.

(9) Isaksson, M. J.; Sitz, G. O. *J. Phys. Chem. A* **1999**, *103*, 2044.

(10) Ahmed, M.; Apps, C. J.; Hughes, C.; Watt, N. E.; Whitehead, J. C. *J. Phys. Chem. A* **1997**, *101*, 1250.
(11) Ahmed, M.; Apps, C. J.; Buesnel, R.; Hughes, C.; Hillier, I. H.; Watt, N. E.; Whitehead, J. C. *J. Phys. Chem. A* **1997**, *101*, 1254.
(12) Apps, C. J.; Watt, N. E.; Whitehead, J. C. *Isr. J. Chem.* **1997**, *37*, 419.
(13) Kroes, G.-J.; Clary, D. C. *J. Phys. Chem.* **1992**, *96*, 7079.
(14) Wang, L.; Clary, D. C. *J. Chem. Phys.* **1996**, *104*, 5663.
(15) Al-Halabi, A.; Kleyn, A. W.; Kroes, G. J. *Chem. Phys. Lett.* **1999**, *307*, 505.
(16) Bolton, K.; Svanberg, M.; Pettersson, J. B. C. *J. Chem. Phys.* **1999**, *110*, 5380.
(17) Bolton, K.; Pettersson, J. B. C. *Chem. Phys. Lett.* **1999**, *312*, 71.
(18) Eisenberg, D.; Kaufmann W., Eds.*; The structure and properties of water*; Oxford University Press: London, 1969, and references therein.
(19) Blackman, M.; Lisgarten, N. D. *Adv. Phys.* **1958**, *7*, 189.
(20) Haynes, D. R.; Tro, N. J.; George, S. M. *J. Phys. Chem.* **1992**, *96*, 8502.
(21) Dowell, L. G.; Rinfret, A. P. *Nature* **1960**, *188*, 1144.
(22) Westley, M. S.; Baratta, G. A.; Baragiola, R. A. *J. Chem. Phys.* **1998**, *108*, 3321.
(23) Jorgensen, W. L.; Chandrasekhar, J.; Madura, J. D.; Impey, R. W.; Klein, M. L. *J. Chem. Phys.* **1983**, *29*, 926.
(24) Cohen, R. C.; Saykally, R. J. *J. Chem. Phys.* **1993**, *98*, 6007.
(25) Tao, F.-M.; Klemperer, W. *J. Chem. Phys.* **1994**, *101*, 1129.
(26) Fredj, E.; Gerber, R. B.; Ratner, M. A. *J. Chem. Phys.* **1998**, *109*, 4833.
(27) Hayward, J. A.; Reimers, J. R. *J. Chem. Phys.* **1997**, *106*, 1518.
(28) DePristo, A. E.; Metiu, H. *J. Chem. Phys.* **1989**, *90*, 1229.
(29) Svanberg, M. *Mol. Phys.* **1997**, *92*, 1085.
(30) Kulginov, D.; Persson, M.; Rettner, C. T.; Bethune, D. S. *J. Phys. Chem.* **1996**, *100*, 7919.
(31) Någård, M. B.; Andersson, P. U.; Marković, N.; Pettersson J. B. C. *J. Chem. Phys.* **1998**, *109*, 10339.
(32) King, M. E.; Nathanson, G. M.; Hanning-Lee, M. A.; Minton, T. K. *Phys. Rev. Lett.* **1993**, *70*, 1026.
(33) Klassen, J. K.; Fiehrer, K. M.; Nathanson, G. M. *J. Phys. Chem. B* **1997**, *101*, 9098.